Autophosphorylation of DNA-PK$_{CS}$ regulates its dynamics at DNA double-strand breaks

Naoya Uematsu,[1] Eric Weterings,[1] Ken-ichi Yano,[1] Keiko Morotomi-Yano,[1] Burkhard Jakob,[2] Gisela Taucher-Scholz,[2] Pierre-Olivier Mari,[3] Dik C. van Gent,[3] Benjamin P.C. Chen,[1] and David J. Chen[1]

[1]Department of Radiation Oncology, University of Texas Southwestern Medical Center, Dallas, TX 75390
[2]Gesellschaft für Schwerionenforschung, Biophysik, D-64291 Darmstadt, Germany
[3]Department of Cell Biology and Genetics, Erasmus Medical Center, University Medical Center, 3000 CA Rotterdam, Netherlands

The DNA-dependent protein kinase catalytic subunit (DNA-PK$_{CS}$) plays an important role during the repair of DNA double-strand breaks (DSBs). It is recruited to DNA ends in the early stages of the nonhomologous end-joining (NHEJ) process, which mediates DSB repair. To study DNA-PK$_{CS}$ recruitment in vivo, we used a laser system to introduce DSBs in a specified region of the cell nucleus. We show that DNA-PK$_{CS}$ accumulates at DSB sites in a Ku80-dependent manner, and that neither the kinase activity nor the phosphorylation status of DNA-PK$_{CS}$ influences its initial accumulation. However, impairment of both of these functions results in deficient DSB repair and the maintained presence of DNA-PK$_{CS}$ at unrepaired DSBs. The use of photobleaching techniques allowed us to determine that the kinase activity and phosphorylation status of DNA-PK$_{CS}$ influence the stability of its binding to DNA ends. We suggest a model in which DNA-PK$_{CS}$ phosphorylation/autophosphorylation facilitates NHEJ by destabilizing the interaction of DNA-PK$_{CS}$ with the DNA ends.

Introduction

DNA double-strand breaks (DSBs) are especially genotoxic DNA lesions because they potentially lead to chromosomal breakage, fragmentation, and translocation. DSBs are commonly caused by exogeneous agents, such as ionizing radiation (IR) or mutagenic chemicals, but are also caused by radicals that emerge during normal cellular metabolism. In addition, DSBs are generated during V(D)J recombination, which is an essential process in the development of functional B and T lymphocytes. It is therefore of vital importance that each cell is equipped with enzymatic machineries that mediate DSB repair.

At least two distinct pathways have evolved that mediate the repair of DSBs: homologous recombination (HR) and nonhomologous end-joining (NHEJ; Critchlow and Jackson, 1998; Kanaar et al., 1998; van Gent et al., 2001; Lieber et al., 2003). NHEJ is considered to be the prevailing pathway during the G0 and G1 phases of the cell cycle in mammalian cells because this repair pathway does not require the presence of an intact DNA template. NHEJ involves juxtaposition of DNA ends by an enzymatic machinery and subsequent ligation. When DNA termini are incompatible or damaged, processing is necessary before ligation can proceed.

Two protein complexes make up the catalytic core of the NHEJ process: the DNA-dependent protein kinase holoenzyme (DNA-PK) and the DNA ligase IV–XRCC4 complex (Lees-Miller and Meek, 2003; Weterings and van Gent, 2004). Ligase IV–XRCC4 mediates ligation of the juxtaposed DNA ends in the final NHEJ step. The DNA-PK holoenzyme consists of the Ku70/80 heterodimer and a 470-kD catalytic subunit (DNA-PK$_{CS}$) with serine/threonine protein kinase activity.

The formation of a kinase-competent DNA-PK complex by Ku70/80 and DNA-PK$_{CS}$ requires simultaneous binding of these enzymes to a DNA terminus (Lees-Miller and Meek, 2003; Weterings and van Gent, 2004). Because Ku70/80 has much higher affinity for DNA ends than DNA-PK$_{CS}$, this heterodimer most likely binds to DNA termini first and subsequently attracts DNA-PK$_{CS}$ toward the DSB.

Many targets for the DNA-PK$_{CS}$ kinase have been found in vitro, but the biological relevance of these observations is unclear in most cases. It is, however, well established that DNA-PK$_{CS}$ has the ability to autophosphorylate itself at a cluster of 6 phosphorylation sites between the Thr2609 and Thr2647 amino acid residues (Douglas et al., 2002), as well as at an additional site outside this cluster, the Ser2056 residue (Chen et al., 2005). This activity possibly leads to alteration of the protein's

N. Uematsu and E. Weterings contributed equally to this paper.

Correspondence to David J. Chen: david.chen@utsouthwestern.edu

Abbreviations used in this paper: DNA-PK, DNA-dependent protein kinase; DNA-PK$_{CS}$, DNA-PK catalytic subunit; DSB, double-strand break; IR, ionizing radiation; NHEJ, nonhomologous end-joining; WT, wild-type.

The online version of this article contains supplemental material.

The Journal of Cell Biology, Vol. 177, No. 2, April 23, 2007 219–229
http://www.jcb.org/cgi/doi/10.1083/jcb.200608077

affinity for DNA and to inactivation of its kinase activity. Such phosphorylation-induced alterations are important during DSB repair in vivo because mutations in the phosphorylation cluster cause severely increased radiation sensitivity and decreased DNA repair (Chan et al., 2002; Ding et al., 2003; Soubeyrand et al., 2003).

Several studies have shown that the presence of DNA-PK_{CS} at DNA ends interferes with efficient ligation, most likely caused by the large dimensions of the protein molecule (Calsou et al., 1999; Weterings et al., 2003; Block et al., 2004; Cui et al., 2005). This inhibition of ligation can be relieved by DNA-PK_{CS} autophosphorylation, indicating that autophosphorylation induces a conformational change in the DNA-PK_{CS} molecule that liberates DNA ends (Weterings et al., 2003; Block et al., 2004; Reddy et al., 2004; Cui et al., 2005). These findings gave rise to the current notion that DNA-PK_{CS} functions as a "gatekeeper," which protects DNA ends from premature processing and ligation, until the two DNA ends are properly juxtaposed and DNA-PK_{CS} autophosphorylation can take place (Weterings and van Gent, 2004).

The spatiotemporal events of this process, however, remain largely unknown. Not much is known about the in vivo dynamics of enzyme–DNA complex formation upon the onset of a DSB event. Several authors have reported the use of microscope-coupled lasers to introduce DNA damage in specified regions of the cell nucleus to address questions concerning the sequential recruitment of different DSB repair enzymes to those damage sites (Kim et al., 2005; Bekker-Jensen et al., 2006). A recent study examined the in vivo recruitment of NHEJ core enzymes to DSBs after the introduction of DNA damage by the use of a pulsed, near-infrared laser (Mari et al., 2006), and it showed that the binding of Ku70/80 to DNA ends is a highly dynamic equilibrium of association and dissociation.

We present a study in which we introduce DSBs in a specific region of the nucleus of living cells by using a pulsed nitrogen laser that was coupled to the epifluorescence path of a fluorescence microscope. This setup enables us to examine the recruitment of YFP-tagged DNA-PK_{CS} to a DSB site in vivo and to follow its behavior throughout the repair process. We monitor the behavior of wild-type (WT) DNA-PK_{CS} and two mutated forms of DNA-PK_{CS} that are either impaired in kinase activity or in the ability to be phosphorylated at 7 phosphorylation sites (the Thr2609-Thr2647 cluster and the Ser2056 residue). These mutations are known to interfere with efficient DSB repair (Kurimasa et al., 1999; Kienker et al., 2000; Chan et al., 2002; Ding et al., 2003; Soubeyrand et al., 2003).

We demonstrate that both WT and mutant DNA-PK_{CS} proteins readily accumulate at the DSB site in a Ku-dependent manner, indicating that neither the kinase activity nor the clustered phosphorylation of DNA-PK_{CS} is important for DNA-PK_{CS} recruitment to DSBs. Impairment of either one of these functions, however, does result in deficient DSB repair. Our data show that DNA-PK_{CS} remains present at unrepaired DSBs for at least 2 h.

By using photobleaching techniques, we demonstrate that DNA-PK_{CS} is not present at DNA ends as a rigid complex, but that there is a dynamic exchange between DNA-bound and free protein. Impairment of phosphorylation/autophosphorylation causes this dynamic exchange to take place at a much lower rate, suggesting that unphosphorylated DNA-PK_{CS} forms a more stable complex with DNA ends than phosphorylated DNA-PK_{CS}. Our findings suggest a model for DNA-PK_{CS}–mediated end-joining in which autophosphorylation is required to destabilize the protein–DNA complex. This destabilization results in accessibility of DNA ends, which, in turn, facilitates ligation. Such a model could comprehensibly explain the radiation-sensitive phenotype of DNA-PK_{CS} autophosphorylation mutants.

Results

DNA-PK_{CS} is recruited to laser-generated DSB sites

To study the spatial and temporal dynamics of DNA-PK_{CS} recruitment to DSBs, we generated a DNA-PK_{CS}–deficient V3 cell line that stably expressed YFP-tagged DNA-PK_{CS}. The expression of tagged DNA-PK_{CS} (verified by Western blot analysis; Fig. S1 A, available at http://www.jcb.org/cgi/content/full/jcb.2006008077/DC1) lead to a considerable decrease in the radiation sensitivity of the V3 cells (Fig. S1 B), indicating that the YFP-tag did not interfere with the function of DNA-PK_{CS} during DSB repair.

We introduced a small area of DNA damage in the nuclei of these cells by using a microirradiation system that utilizes a 365-nm pulsed nitrogen laser. Directly after microirradiation, YFP-DNA-PK_{CS} started to accumulate at the damaged region (Fig. 1, A and B). We verified that the laser treatment generated DSBs by TUNEL labeling and by staining with an antibody that recognized γH2AX. DNA-PK_{CS} clearly colocalized with TUNEL and γH2AX in the microirradiated area (Fig. 1 A), demonstrating that DNA-PK_{CS} localizes in vivo at laser-induced DSB sites.

To estimate the number of DSBs that was produced during microirradiation, we compared the DNA-PK_{CS} accumulation that was caused by our laser-system with the DNA-PK_{CS} accumulation that was caused by an already calibrated microirradiation system (Mari et al., 2006). In brief, we treated YFP-DNA-PK_{CS}–expressing cells with either our 365-nm laser system or with the 800-nm multiphoton laser system used by Mari et al. (2006), which is known to introduce between 1,000 and 1,500 DSBs. We then measured and compared the fluorescence intensity of the accumulated YFP-DNA-PK_{CS} at the microirradiated sites, which is correlated in a linear fashion to the number of induced DSBs. After correction for the differences in accumulation area size, we found that the fluorescence intensity of the accumulated DNA-PK_{CS} was 2.5-fold higher after microirradiation with the 365-nm laser than after irradiation with the 800-nm laser. From this, we infer that ∼3,000 DSBs are produced at the beam-focus of our pulsed 365-nm laser (see Materials and methods for details).

To study the kinetics of DNA-PK_{CS} accumulation after microirradiation with the 365-nm laser, we performed time-lapse imaging. Recruitment of YFP-DNA-PK_{CS} to DSB sites was observed as early as 2 s after microirradiation, and the

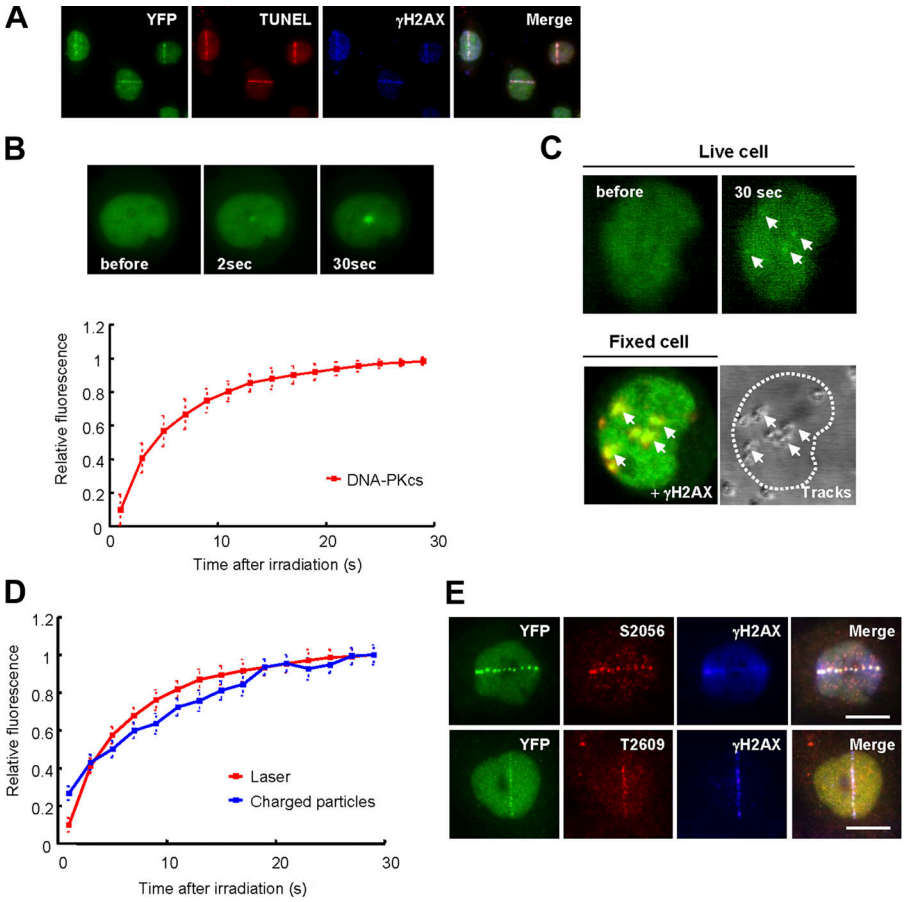

Figure 1. **DNA-PK$_{CS}$ accumulates at DSB sites induced by laser microirradiation and heavy charged particles.** (A) TUNEL labeling (red) and γH2AX immunostaining (blue) of YFP-DNA-PK$_{CS}$–expressing V3 cells after microirradiation. (B, top) Time-lapse imaging of YFP-DNA-PK$_{CS}$–expressing V3 cells before and after microirradiation. (bottom) Kinetics of relative fluorescence of YFP-DNA-PK$_{CS}$ accumulation at the DSB site after microirradiation. Each data point is the average of 10 independent measurements. Error bars represent the SD. (C) Time-lapse imaging of YFP-DNA-PK$_{CS}$–expressing V3 cells before and after irradiation with uranium-charged particles. (top) Living cells before and 30-s after irradiation. (bottom left) Merged γH2AX staining. (bottom right) Tracks of the uranium particles through the cell nucleus. Arrows point to DNA-PK$_{CS}$ accumulation sites. (D) Kinetics of DNA-PK$_{CS}$ accumulation at the DSB site after microirradiation (red) or uranium irradiation (blue). Each data point is the average of 10 independent measurements. Error bars represent the SD. (E) Coimmunostaining of microirradiated YFP-DNA-PK$_{CS}$–expressing V3 cells with γH2AX antibody (blue) and phosphospecific antibodies to the Ser-2056 or Thr-2609 amino acid residues of DNA-PK$_{CS}$ (red). Bar, 10 μm.

intensity of the YFP signal rapidly increased during the first 20 s (Fig. 1 B). To verify whether the kinetics of DNA-PK$_{CS}$ accumulation at laser-induced DSB sites are comparable to those at IR-induced DSB sites, we exposed our YFP-DNA-PK$_{CS}$ cells to charged uranium particles and observed immediate DNA-PK$_{CS}$ accumulation. The accumulation pattern matched the pattern of the uranium particles and colocalized with γH2AX (Fig. 1 C). The fast DNA-PK$_{CS}$ accumulation at the uranium-induced DSB sites resembled the DNA-PK$_{CS}$ accumulation at laser-generated DSB sites (Fig. 1 D), suggesting that the response of DNA-PK$_{CS}$ to both types of induced damage is comparable.

In addition, we investigated the phosphorylation status of accumulated DNA-PK$_{CS}$ in the microirradiated area. We have previously shown that IR induces phosphorylation/autophosphorylation of the Ser2056 and Thr2609 amino acid residues of DNA-PK$_{CS}$ (Chan et al., 2002; Chen et al., 2005). Immunostaining with phosphospecific antibodies revealed that both the Ser-2056 and Thr-2609 residues were phosphorylated in the microirradiated region (Fig. 1 E), indicating that the laser-induced DNA lesions are capable of inducing a repair response that involves DNA-PK$_{CS}$ phosphorylation/autophosphorylation.

Ku80 is essential for the recruitment of DNA-PK$_{CS}$ at DSB sites

Many in vitro studies have shown that the Ku70/80 heterodimer directs DNA-PK$_{CS}$ to DNA ends and stabilizes the DNA–DNA-PK$_{CS}$ interaction (Smith and Jackson, 1999). To investigate whether the recruitment of DNA-PK$_{CS}$ to DSB sites is dependent on the Ku protein in vivo, we generated a Ku80-deficient Xrs6 cell line that stably expressed YFP-DNA-PK$_{CS}$. After microirradiation of the nuclei of these cells, we did not observe any accumulation of DNA-PK$_{CS}$, although γH2AX staining confirmed that DSBs were introduced in the irradiated area (Fig. 2 A). Continued time-lapse imaging for a period of 2 h after microirradiation did not reveal any accumulation of DNA-PK$_{CS}$ (not depicted).

In addition, we complemented our YFP-DNA-PK$_{CS}$–expressing Xrs6 cell line with human Ku80, which restored the expression level of Ku80 protein and decreased the radiosensitivity of these cells to the same level as that of the parental AA8 cell line (Fig. S2, A and B, available at http://www.jcb.org/cgi/content/full/jcb.200608077/DC1). After microirradiation of these complemented cells, we observed immediate accumulation of DNA-PK$_{CS}$ (Fig. 2 B). The kinetics of this accumulation were very similar to those observed in V3 cells (Fig. 2 C). These data demonstrate that Ku80 is essential for the recruitment of DNA-PK$_{CS}$ to DSB sites in vivo.

To examine whether the phosphorylation of DNA-PK$_{CS}$ also takes place in a Ku-dependent manner in our system, we immunoprecipitated DNA-PK$_{CS}$ from Ku-deficient, YFP-DNA-PK$_{CS}$–expressing Xrs6 cells and from YFP-DNA-PK$_{CS}$–expressing V3 cells after IR treatment with gamma radiation. Subsequently, we performed a Western blot analysis, using phosphospecific antibodies against the Ser-2056 residue of DNA-PK$_{CS}$.

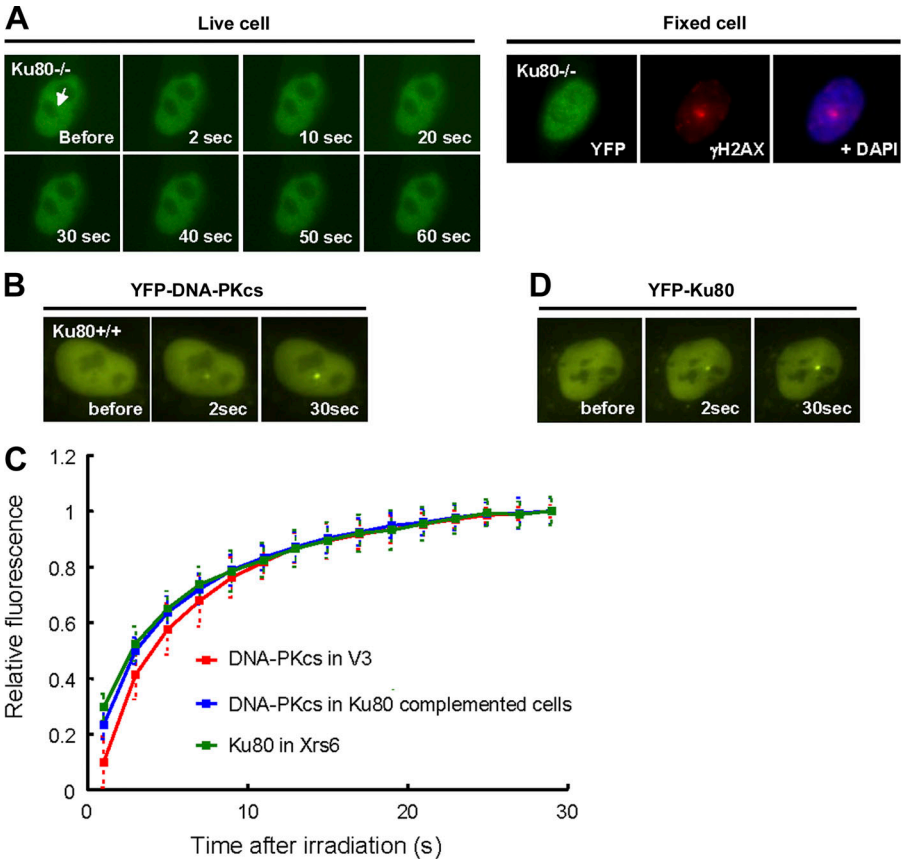

Figure 2. **Ku80 is essential for the recruitment of DNA-PK$_{CS}$ to DSB sites in vivo.** (A, left) Time-lapse imaging of YFP-DNA-PK$_{CS}$–expressing Xrs6 cells before and after microirradiation. (right) γH2AX staining. Arrow points to the microirradiated site. (B) Time-lapse imaging of Ku80-complemented, YFP-DNA-PK$_{CS}$–expressing Xrs6 cells before and after microirradiation. (C) Kinetics of DNA-PK$_{CS}$ and Ku80 accumulation at the DSB site after microirradiation. Red, YFP-DNA-PK$_{CS}$ in V3 cells; blue, YFP-DNA-PK$_{CS}$ in Ku80-complemented Xrs6 cells; green, YFP-Ku80 in Xrs6 cells. Each data point is the average of 10 independent measurements. Error bars represent the SD. (D) Time-lapse imaging of YFP-Ku80–expressing Xrs6 cells before and after microirradiation.

Ser-2056 phosphorylation clearly took place after IR treatment in the V3 cells, but the Ku-deficient cell line did not show any detectable Ser-2056 phosphorylation (Fig. S2 C). From these data and the previously reported notion that the phosphorylation of Thr2609 does not take place in Ku-deficient cells (Falck et al., 2005), we conclude that phosphorylation/autophosphorylation of DNA-PK$_{CS}$ is a Ku-dependent process.

To analyze the kinetics of Ku80 accumulation at DSB sites, we generated YFP-Ku80–expressing Xrs6 cells and subjected those to microirradiation. Accumulation of Ku80 at DSB sites was observed within 2 s after microirradiation (Fig. 2 D) and the kinetics of Ku80 accumulation were identical to those of DNA-PK$_{CS}$ accumulation (Fig. 2 C). These data suggest that Ku80 and DNA-PK$_{CS}$ show similar spatial and temporal behavior at DSB sites immediately after the damage induction.

Impairment of the kinase activity or clustered phosphorylation of DNA-PK$_{CS}$ leads to reduced DSB repair and the maintained presence of DNA-PK$_{CS}$ at DSB sites

It has previously been shown that the kinase activity of DNA-PK$_{CS}$ is essential during NHEJ-mediated DSB repair in mammalian cells (Kurimasa et al., 1999; Kienker et al., 2000). Because mutation of DNA-PK$_{CS}$ phosphorylation sites is also known to interfere with DSB repair, clustered phosphorylation of DNA-PK$_{CS}$ is likely to play an important role during NHEJ (Chan et al., 2002; Ding et al., 2003; Chen et al., 2005; Cui et al., 2005). To test whether kinase activity and clustered phosphorylation of DNA-PK$_{CS}$ are important for its recruitment to DSB sites, we generated two V3 cell lines that stably expressed YFP-tagged mutant forms of DNA-PK$_{CS}$. In one mutant form (KD), we impaired the kinase ability (Kurimasa et al., 1999). In the other mutant (7A), we substituted all of the 7 major phosphorylation sites (Thr2609-Thr2647 and Ser2056) with alanine residues, impairing phosphorylation of these sites (Fig. 3 A). Cellular expression of both mutant proteins was verified by Western blot analysis (Fig. S1 A).

Upon microirradiation, we observed accumulation of both the KD and the 7A variant of DNA-PK$_{CS}$ colocalizing with γH2AX (Fig. 3 B). Accumulated KD protein proved to be phosphorylated at the Thr2609 and Thr2647 amino acid residues, but not at the Ser2056 residue (Fig. 3 B). This is consistent with our previous finding that Ser2056 is an autophosphorylation site and that phosphorylation of this residue therefore requires the DNA-PK$_{CS}$ kinase activity (Chen et al., 2005). The Thr2609 and Thr2647 residues, which were previously reported to be autophosphorylation sites (Chan et al., 2002; Ding et al., 2003), apparently do not require the DNA-PK$_{CS}$ kinase to be phosphorylated. It has recently been shown that phosphorylation of these two residues can also be mediated by ATM (Chen et al., 2007). As expected, the 7A mutant did not display phosphorylation of Thr2609, Thr2647, or Ser2056 (Fig. 3 B).

Time-lapse imaging showed that the accumulation kinetics of the 7A and KD proteins are indistinguishable from those observed with WT DNA-PK$_{CS}$ (Fig. 3 C). In both mutant cells, the intensity of the fluorescent signal in the microirradiated

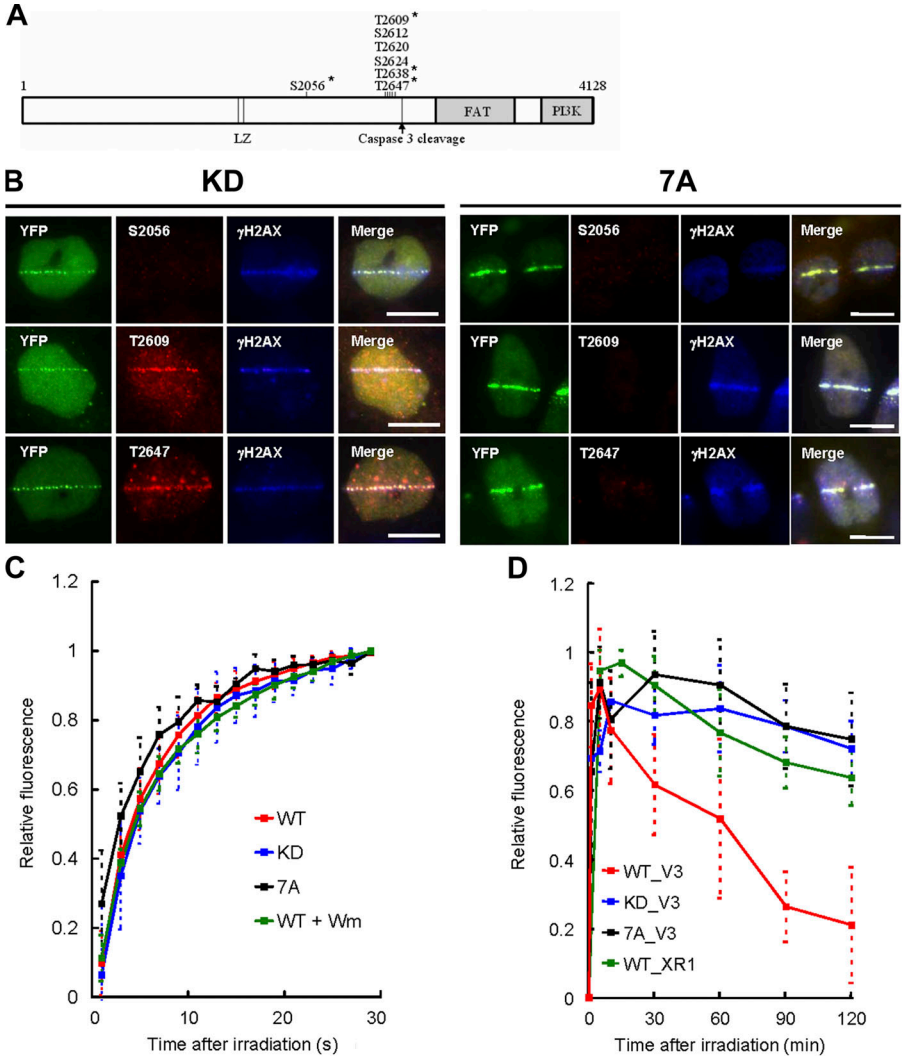

Figure 3. **Impairment of either kinase activity or clustered phosphorylation of DNA-PK$_{CS}$ leads to reduced DSB repair and the maintained presence of DNA-PK$_{CS}$ at DSB sites.** (A) Summary of known in vitro and in vivo phosphorylation sites of DNA-PK$_{CS}$. Asterisks indicate in vivo sites of IR-induced phosphorylation. The modifications we made in our 7A DNA-PK$_{CS}$ mutant are as follows: S2056A, T2609A, S2612A, T2620A, S2624A, T2638A, and T2647A. (B) Coimmunostaining of KD (left) and 7A cells (right), using phosphospecific antibodies against the S2056, T2609, or T2647 amino acid residues of DNA-PK$_{CS}$ (red) and against γH2AX (blue). Bars, 10 μm. (C) Initial accumulation kinetics of WT, KD, 7A, and WT + wortmannin at the DSB site after microirradiation. Each data point is the average of 10 independent measurements. Error bars represent the SD. (D) 2-h time-course after microirradiation, showing the kinetics of WT, 7A, and KD in V3 cells and WT in XR1 cells. Each data point is the average of 10 independent measurements. Error bars represent the SD.

area increased rapidly during the first 20 s and reached a level that is identical to that found in WT cells. In addition, we demonstrated that pretreatment of WT cells with 30 μM of the phosphoinositide 3 kinase inhibitor wortmannin did not alter the accumulation kinetics of DNA-PK$_{CS}$ (Fig. 3 C). Collectively, these data show that the kinase activity and clustered phosphorylation of the DNA-PK$_{CS}$ protein are dispensable for its initial localization at DSB sites.

After establishing the accumulation kinetics of both mutants at DSB sites, we performed time-lapse imaging experiments for a period of 2 h after laser irradiation. This allowed us to measure any decrease in the fluorescence intensity of the accumulation area in time. Interestingly, we observed significant differences between the behavior of WT and mutant proteins at the DSB site (Fig. 3 D). The fluorescence intensity of the accumulation area in WT cells decreased to 20% of the maximum level in a 2-h period, whereas the intensity of the accumulation area in KD and 7A cells only dropped to 80% of the maximum level in the same period of time. These results demonstrate that impairment of either DNA-PK$_{CS}$ kinase activity or clustered phosphorylation results in a maintained overall presence of DNA-PK$_{CS}$ at the DSB sites.

The slow decrease of the fluorescence intensity of the accumulation area in mutant cells most likely reflects the inability of these cells to quickly repair the introduced DSBs because it is known that 7A and KD mutants display deficient DSB repair (Kurimasa et al., 1999; Kienker et al., 2000; Chan et al., 2002; Ding et al., 2003; Soubeyrand et al., 2003). To verify this, we generated an XRCC4-deficient (XR1) cell line that expressed YFP-tagged WT DNA-PK$_{CS}$. Because XR1 cells are unable to efficiently repair DSBs (Li et al., 1995), we expected the presence of DNA-PK$_{CS}$ to be maintained at the DSB site. Indeed, the fluorescence intensity of the accumulation area decreased only slightly in a 2-h period and reached a level that was comparable to that of KD and 7A (Fig. 3 D). These results show that the maintained presence of DNA-PK$_{CS}$ at DSB sites is correlated to deficient DSB repair, independent of the cause of the deficient DSB repair.

We subsequently examined the behavior of DNA-PK$_{CS}$ mutants in which we impaired phosphorylation of a single site within the phosphorylation cluster. Because phosphorylation of both Thr2609 and Ser2056 is thought to be important for DSB repair via the NHEJ pathway (Chan et al., 2002; Ding et al., 2003; Chen et al., 2005; Cui et al., 2005), we generated

V3 cell lines that stably expressed YFP-tagged mutant forms of DNA-PK$_{CS}$ that could not be phosphorylated at those sites (Fig. 3 A). Cellular expression of both mutant forms of DNA-PK$_{CS}$ was verified by Western blot analysis (Fig. S3, available at http://www.jcb.org/cgi/content/full/jcb.2006008077/DC1).

We observed rapid accumulation of both phospho mutants at laser-induced DSB sites colocalizing with γH2AX (Fig. 4 A). As expected, the accumulation kinetics of S2056A and T2609 were identical to those of WT DNA-PK$_{CS}$ (Fig. 4 B). Although the S2056A protein disappeared slower from the DSB site than WT protein, neither mutant showed a behavior comparable to that of 7A (Fig. 4 C). It is very likely that the complete cluster of phosphorylation sites has to be substituted to observe a long, sustained presence of DNA-PK$_{CS}$ at the DSB sites.

Kinase activity and clustered phosphorylation of DNA-PK$_{CS}$ influence the exchange rate between DNA-bound and free DNA-PK$_{CS}$ at DSB sites

We subsequently examined the stability of the protein–DNA complexes that are formed by WT DNA-PK$_{CS}$ and the DNA-PK$_{CS}$ mutants at DSB sites by photobleaching the region of DNA-PK$_{CS}$ accumulation. Photobleaching took place 10 min after DSB induction, thus allowing for maximum accumulation of DNA-PK$_{CS}$ at the DSB site. We then monitored FRAP at regular intervals for a period of 10 min. As shown in Fig. 5 A, we observed recovery of fluorescence after photobleaching the area of DNA damage in WT DNA-PK$_{CS}$ cells, demonstrating that DNA-PK$_{CS}$ is not attached to DSBs in a rigid complex, but that there is a dynamic exchange between DNA-bound and free DNA-PK$_{CS}$.

In addition, we found that recovery of fluorescence after photobleaching occurred at a much faster rate in WT cells than in KD and 7A mutant cells (Fig. 5 B). In WT cells, fluorescence recovery reached a maximum of ∼60% of the prebleach intensity after 300 s. In contrast, fluorescence recovery in both mutants remained incomplete at that time. The 7A mutant recovered ∼30% of the prebleach intensity after 300 s, whereas the KD mutant displayed a remarkably low recovery of 10% at that time. These results clearly show that the dynamic exchange of DNA-bound protein with free protein is much faster in WT cells than in 7A or KD cells, and therefore this dynamic exchange must be influenced by both the kinase activity and the clustered phosphorylation of DNA-PK$_{CS}$.

We subsequently studied the FRAP dynamics of the WT, 7A, and KD proteins in an area of the cell nucleus where no DNA damage was present. The dynamics of WT, 7A, and KD proved to be identical under these conditions, showing that the 7A and KD mutants do not display an intrinsic tendency to recover slower than WT DNA-PK$_{CS}$ in the absence of DNA damage (Fig. 5 C). Maximum recovery of both WT and mutant DNA-PK$_{CS}$ in the undamaged area was reached in <10 s, which is 30 times faster than the recovery of WT DNA-PK$_{CS}$ at DSB

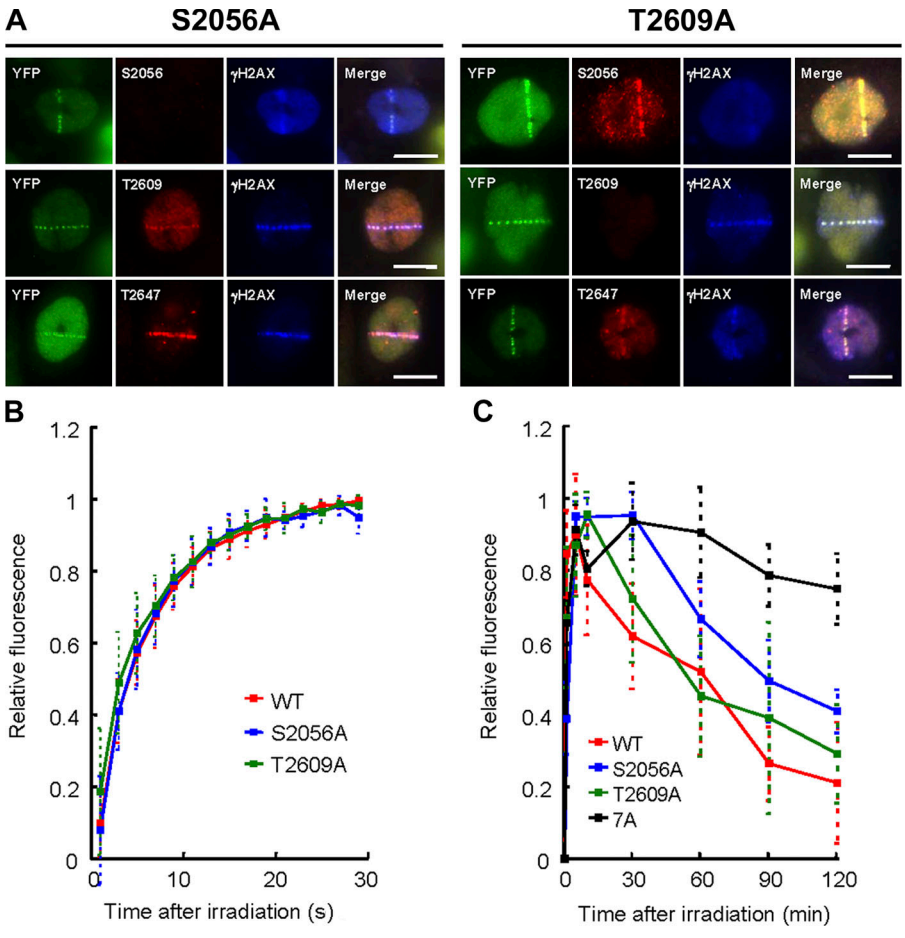

Figure 4. **Mutation of the phosphorylation cluster of DNA-PK$_{CS}$ leads to longer maintained presence of DNA-PK$_{CS}$ at DSB sites than mutation of single phosphorylation sites.** (A) Co-immunostaining of microirradiated S2056A and T2609A cells with phosphospecific antibodies against the S2056, T2609, or T2647 amino acid residues of DNA-PK$_{CS}$ (red) and against γH2AX (blue). Bars, 10 μm. (B) Initial accumulation kinetics of WT, S2056A, and T2609A at a DSB site after microirradiation. Each data point is the average of 10 independent measurements. Error bars represent the SD. (C) 2-h time-course after microirradiation, showing the kinetics of WT, 7A, S2056A, and T2609A. Each data point is the average of 10 independent measurements. Error bars represent the SD.

sites (300 s). The much prolonged recovery rate of DNA-PK$_{CS}$ at DSB sites thus reflects the binding of DNA-PK$_{CS}$ to the DNA ends. Henceforth, the difference in recovery rates between WT, KD, and 7A at the DSB site (Fig. 5 B) must reflect a difference in the stability of the DNA–protein species.

Discussion

Laser-mediated introduction of DSBs in vivo

To effectively study the response of the DNA-PK holoenzyme to the onset of DSBs in vivo, we needed a system that could quickly and reliably induce DSBs in a small region of the cell nucleus. We chose to use a 365-nm laser system, which is known for its ability to generate DNA damage in a controlled fashion (Lan et al., 2004, 2005). The type and amount of DNA damage that is introduced by this laser can be controlled by adjusting the laser output intensity and the pulse frequency (Lan et al., 2005). A previous study has demonstrated the recruitment of DSB repair proteins (NBS1, BRCA1, RAD52, and WRN) toward regions of the cell nucleus that were treated with this laser system, indicating that the system is capable of generating DSBs (Lan et al., 2005). In addition, we show that the laser system generates DNA ends and that microirradiated areas colocalize with γH2AX, thereby demonstrating the formation of DSBs.

It has recently been suggested that visible accumulation of Ku70 and DNA-PK$_{CS}$ at DNA damage sites is highly dependent on the output intensity of the laser that creates the DNA damage (Bekker-Jensen et al., 2006). In this study, a relatively mild laser treatment of BrdU-sensitized cells did not suffice to induce visible accumulation of both NHEJ enzymes, whereas treatment of nonsensitized cells with higher output intensity did result in detectable accumulation of DNA-PK$_{CS}$ and Ku70 at the damage site. The authors of this study theorize that the use of such high laser output intensity leads to a widespread chromosomal damage that saturates the cellular capacity to repair the lesions. Henceforth, they infer that high-powered lasers cause too much collateral damage to produce meaningful results (Bekker-Jensen et al., 2006). Our results, however, suggest that repair of the lesions that are generated with our laser system does take place efficiently. This is supported by the fact that accumulated WT DNA-PK$_{CS}$ disappears much faster from the DSB site in repair-proficient cells than in repair-deficient cells (Fig. 3 D). A recent study, in which cells were exposed to a comparable number of DSBs, showed conclusively that these cells were still able to complete cell division (Mari et al., 2006). In addition, we would like to stipulate that the recruitment of DNA-PK$_{CS}$ in our system fully depends on the presence of Ku, ruling out the possibility of artificial, aspecific aggregation.

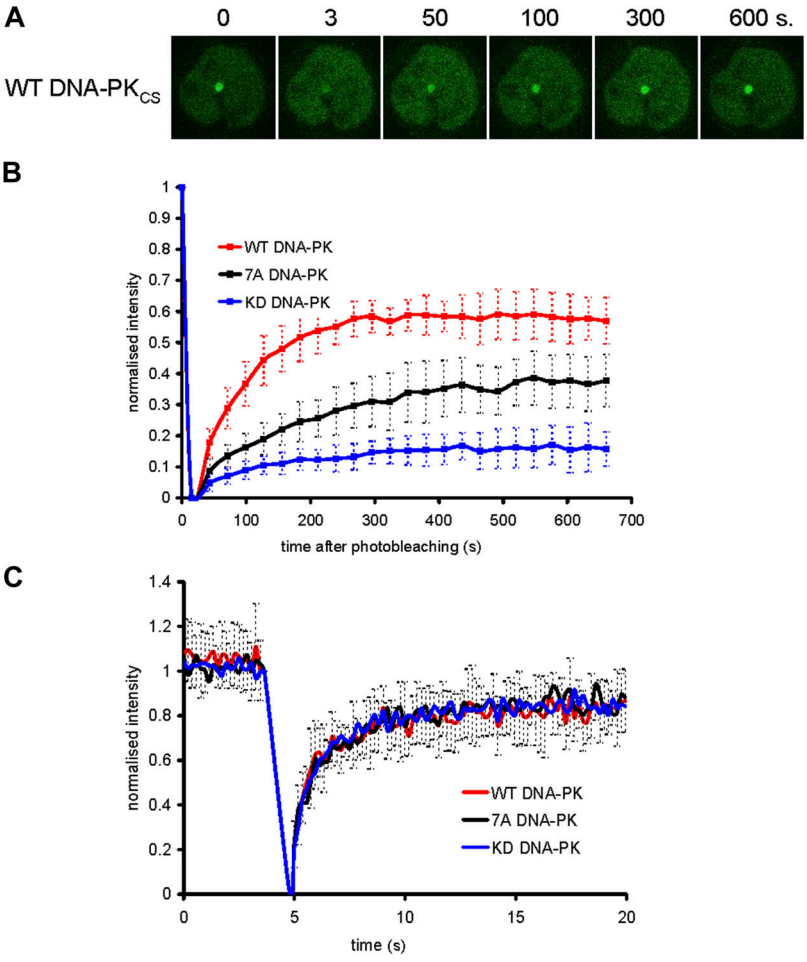

Figure 5. **Kinase activity and clustered phosphorylation of DNA-PK$_{CS}$ influence the exchange rate between DNA-bound and free DNA-PK$_{CS}$ at DSB sites.** (A) Time-lapse imaging of WT cells after photobleaching of the DSB site. The first picture (t = 0 s) is the prebleach situation, the second picture (t = 3 s) was taken immediately after photobleaching. (B) FRAP curves of WT DNA-PK$_{CS}$, 7A, and KD at the DSB site. Each data point is the average of 15 independent, normalized measurements. Error bars represent the SD. Prebleach intensity levels were normalized to 1, postbleach intensity levels were normalized to 0. (C) FRAP curves of WT DNA-PK$_{CS}$, 7A, and KD in an area of the cell nucleus where no DNA damage is present. Each data point is the average of 10 independent, normalized measurements. Error bars represent the SD. Prebleach intensity levels were normalized to 1, postbleach intensity levels were normalized to 0.

Ku80 is essential for recruitment of DNA-PK$_{CS}$ to DNA DSBs

It is generally assumed that the Ku70/80 heterodimer is the first NHEJ factor to bind to a broken DNA strand and that DNA-PK$_{CS}$ is subsequently attracted to the DSB sites (Chen et al., 1996; Singleton et al., 1999). Recent studies have demonstrated that conserved C-terminal sequence motifs in Ku80 have the ability to interact with DNA-PK$_{CS}$ (Falck et al., 2005). However, these in vitro studies do not form direct evidence for Ku80's ability to recruit DNA-PK$_{CS}$ to DSB sites. Some experiments have even suggested that DNA-PK$_{CS}$ is able to bind to DNA ends in the absence of Ku70/80 (Hammarsten and Chu, 1998; Merkle et al., 2002). We directly demonstrate that DNA-PK$_{CS}$ does not visibly accumulate at induced DSB sites in Ku80-deficient cells. Complementing these cells with Ku80 restores the ability of DNA-PK$_{CS}$ to accumulate. Collectively, our findings indicate that recruitment of DNA-PK$_{CS}$ to DSB sites is mediated by Ku80 in vivo. In addition, we show that not only the recruitment but also the phosphorylation of (the autophosphorylation Ser-2056 residue of) DNA-PK$_{CS}$ is Ku dependent. This provides further evidence for the notion that the assembly of a kinase-competent DNA–PK complex relies on the presence of Ku80.

Kinase activity and clustered phosphorylation of DNA-PK$_{CS}$ influence the exchange rate between DNA-bound and free DNA-PK$_{CS}$ at DSB sites

The experiments presented in this paper demonstrate that kinase- and phosphorylation-impaired DNA-PK$_{CS}$ mutants readily accumulate at DSB sites, but that their presence at the DSB site is maintained for a significantly longer period of time than observed for WT DNA-PK$_{CS}$. This most likely reflects the inability of these mutant cells to repair DSBs. Apparently, the presence of DNA-PK$_{CS}$ is maintained at unrepaired DNA breaks in general because even WT DNA-PK$_{CS}$ hardly disappears from the DSB site in repair-deficient XR1 cells. Clearly, in the latter case, this is not caused by any mutation in the DNA-PK$_{CS}$ molecule. Hence, we must conclude that whatever the cause of the deficient repair may be, DNA-PK$_{CS}$ will be present at the remaining DNA ends. But what causes diminished repair in the 7A and KD mutants?

Our photobleaching experiments show that the presence of DNA-PK$_{CS}$ at DNA ends is not rigid, but that it is, in fact, a dynamic equilibrium between dissociating DNA-bound molecules and associating free molecules. These findings are in agreement with recent observations of the in vivo behavior of Ku80 at DSB sites (Mari et al., 2006). The 7A and KD mutations cause a dramatic decrease in the exchange rate of bound and free molecules. In other words, these mutant DNA-PK$_{CS}$ molecules are more stably bound to DNA ends than WT molecules. Obviously, there is still exchange between bound and free protein, but at a much lower rate than observed for WT DNA-PK$_{CS}$. Because inhibition of either one of the two requirements for DNA-PK$_{CS}$ autophosphorylation (either an active kinase domain or the ability to be phosphorylated) changes this exchange rate, it is reasonable to assume that autophosphorylation changes the stability of the DNA-PK$_{CS}$–DNA complex.

Biochemical experiments have demonstrated that unphosphorylated DNA-PK$_{CS}$ blocks DNA ends, and thereby inhibits efficient ligation (Weterings et al., 2003; Block et al., 2004). This ligation block can be relieved by DNA-PK$_{CS}$ autophosphorylation, which induces a conformational change in the DNA–protein complex that liberates the DNA ends. Combined with our in vivo data on exchange rates, these data suggest a comprehensive model for the role of DNA-PK$_{CS}$ autophosphorylation during NHEJ (Fig. 6). In WT cells, unphosphorylated DNA-PK$_{CS}$ binds to the ends of a broken DNA strand. The dynamic dissociation/reassociation equilibrium of this unphosphorylated molecule will most likely be comparable to that of the 7A or KD mutants, which is a very slow rate of exchange. Hence, the DNA end will usually be occupied by a DNA-PK$_{CS}$ molecule. This effectively protects the DNA ends from (premature) processing, degradation by nucleases, or undesirable ligation. Subsequently, when the DNA ends are correctly juxtaposed (Cui et al., 2005), the DNA-PK$_{CS}$ molecules will autophosphorylate each other. This induces a change in the dynamic association/dissociation rate that, in effect, liberates the DNA ends.

It is not completely clear how we should envision this conformational change, but our FRAP data suggests that the

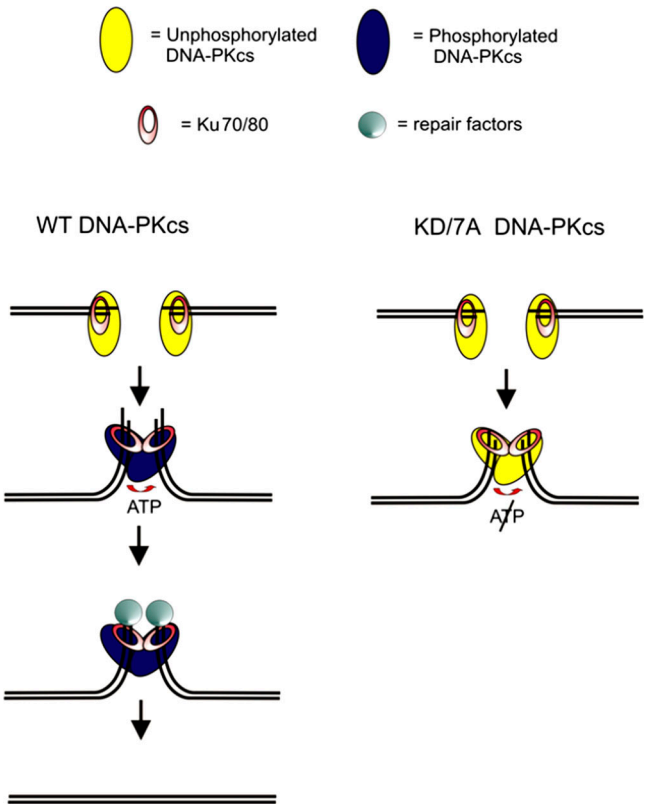

Figure 6. **A model for the DNA-PK$_{CS}$ autophosphorylation process.** The model is based on data presented in this paper, and on previously reported experiments. After the onset of a DSB, the DNA ends are recognized by the Ku70/80 heterodimer, which attracts unphosphorylated DNA-PK$_{CS}$. The dynamic exchange between DNA-bound and free DNA-PK$_{CS}$ takes place at a low rate as long as DNA-PK$_{CS}$ remains unphosphorylated. This protects the DNA ends from premature processing or ligation. After tethering of the broken DNA ends, DNA-PK$_{CS}$ autophosphorylation takes place. This effectively liberates the DNA ends, thereby enabling processing and ligation.

exchange of DNA-bound DNA-PK_{CS} with free DNA-PK_{CS} is (relatively) rapid in a setting that enables DNA-PK_{CS} phosphorylation/autophosphorylation. The window of time between dissociation of a bound molecule and reassociation of a new molecule may not differ between the unphosphorylated state and the phosphorylated state, but an exchange event will take place more frequently in the phosphorylated state. Hence, the DNA ends are more exposed to other repair factors in the latter case.

In view of the aforementioned model, it is interesting to note that the kinase-impaired mutant of DNA-PK_{CS} is phosphorylated at the Thr2609 and Thr2647 residues (Fig. 3 B) and still displays an exchange rate that is lower than that of the 7A mutant, in which none of those residues are phosphorylated (Fig. 5 B). This discrepancy can be explained by taking into account that DNA-PK_{CS} has several autophosphorylation sites that are functional in the 7A mutant, but that will not be phosphorylated in KD cells. For example, we did not mutate the Ser3205 residue that has previously been identified as an autophosphorylation site (Douglas et al., 2002). This site can still be phosphorylated in the 7A mutant, but not in the KD mutant.

It is reasonable to assume that other DNA-PK–mediated processes are important for NHEJ as well. As a consequence, impairment of the DNA-PK_{CS} kinase activity or clustered phosphorylation may influence the NHEJ process in other ways than merely by influencing the stability of the DNA-PK_{CS}–DNA complex. Recently, it has been shown that autophosphorylation is important for the activation of the processing factor Artemis (Goodarzi et al., 2006). Inhibition of Artemis activation could lead to incorrect or absent processing of the DNA ends, which in turn may affect ligation efficiency. In addition, the DNA-PK_{CS} kinase activity has been demonstrated to play a role in the phosphorylation of XRCC4. Alternatively, DNA-PK_{CS} (like ATM) may be required for downstream signaling after the initial detection of DNA damage. All of these possibilities require further investigation.

In conclusion, we demonstrate that DNA-PK_{CS} phosphorylation/autophosphorylation facilitates NHEJ by destabilizing the DNA–DNA-PK_{CS} complex, which, in turn, enables efficient ligation. This is a comprehensive explanation for the reduced repair efficiency that is observed in DNA-PK_{CS} autophosphorylation mutants, although it is possible that other factors contribute to this phenotype.

Materials and methods

Cell culture

CHO cell lines AA8 (WT), V3 cells (defective in DNA-PKcs expression; Whitmore et al., 1989), and Xrs6 cells (defective in Ku80 expression; Denekamp et al., 1989) were maintained at 37°C in α-minimum Eagle's medium with 10% FCS, 100 units/ml penicillin, and 100 μg/ml streptomycin (HyClone). Stable cell lines expressing YFP-tagged DNA-PK_{CS} or YFP-tagged Ku80 were maintained with 400 μg/ml of G418.

Fluorescent immunostaining and antibodies

Fluorescent immunostaining was performed as previously described (Chen et al., 2005). In brief, the irradiated cells were fixed with cold methanol for 20 min on ice and permeabilized for 10 min in PBS containing 0.5% Triton X-100. After blocking with PBS containing 5% BSA for 20 min, the cells were subjected to incubation with the primary antibodies. Anti-pS2056 and -pT2647 polyclonal antibodies and anti-pT2609 and -γH2AX monoclonal antibodies were generated as described previously (Chan et al., 2002; Chen et al., 2005; Yajima et al., 2006). Anti-γH2AX polyclonal antibody was purchased from Cell Signaling Technology. Secondary antibodies (anti–mouse or–rabbit conjugated with Alexa Fluor 488/350 or rhodamine) were purchased from Invitrogen. DNA ends in irradiated cells were labeled with TAMRA-dCTP (Roche) according to the manufacturer's specifications.

Laser microirradiation and imaging

DSBs were introduced in the nuclei of cultured cells by microirradiation with a pulsed nitrogen laser (Spectra-Physics; 365 nm, 10 Hz pulse) as previously described (Lan et al., 2004, 2005). The laser system was directly coupled (Micropoint Ablation Laser System; Photonic Instruments, Inc.) to the epifluorescence path of the microscope (Axiovert 200M [Carl Zeiss MicroImaging, Inc.] for immunostaining imaging or time-lapse imaging and confocal LSM 510 Meta [Carl Zeiss MicroImaging, Inc.] for FRAP analysis) and focused through a Plan-Apochromat 63×/NA 1.40 oil immersion objective (Carl Zeiss MicroImaging, Inc.). The output of the laser power was set at 60% of the maximum, which is the minimal dose required to induce detectable accumulation of YFP-tagged DNA-PK_{CS} in living cells. Immunostaining and time-lapse images were taken with an AxioCam HRm (Carl Zeiss MicroImaging, Inc.). During microirradiation, imaging, or analysis, the cells were maintained at 37°C in 35-mm glass-bottom culture dishes (MatTek Cultureware). The growth medium was replaced by CO_2-independent medium (Invitrogen) before analysis.

Number of DSBs introduced by laser microirradiation

To estimate the number of DSBs that were induced by microirradiation, we compared the DNA-PK_{CS} accumulation that was caused by our 365-nm laser system with the DNA-PK_{CS} accumulation that was caused by a previously calibrated system (Mari et al., 2006). Mari et al. (2006) used an 800-nm multiphoton laser to induce DNA damage. They estimated the biological impact of their microirradiation system by comparing the fraction of Ku80 that was immobilized after microirradiation with the fraction of Ku80 that was immobilized after exposure to gamma irradiation. From these data, they calculated their system to induce between 1,000 and 1,500 DSBs (for a given laser power output, target surface, and exposure duration).

We microirradiated several YFP-DNA-PK_{CS}–expressing V3 cells with either our 365-nm laser system or with the microirradiation system used by Mari et al. (2006; both systems are based on LSM 510 confocal microscopes, set to provide comparable background and fluorescence intensity levels). Using the same microirradiation system that was used by Mari et al. (2006; facility of the Erasmus Medical Center, Rotterdam, Netherlands) and following the same protocol, a small disk within the nucleus was irradiated with a pulsed 800-nm laser. Allowing for accumulation of YFP-DNA-PK_{CS}, the average fluorescence in the disc was measured using the LSM 510 software and compared with the same quantity measured in nuclei that were exposed to our 365-nm laser. After subtraction of the average nuclear fluorescence intensity (undamaged area), we found the average fluorescence intensity at the 365-nm microirradiated region to be ∼7 times higher than at the 800-nm microirradiated region (223 arbitrary units for the 800-nm laser versus 1,576 arbitrary units for the 365-nm laser). We subsequently measured the dimensions of the accumulation areas and found those to be 1.7 μm^2 for the 365-nm spot and 4.9 μm^2 for the 800-nm spot (measuring slices of identical thickness in the z direction), which is a 2.8-fold difference. Taking into account these differences in the accumulation areas produced by the laser-systems, we estimated that the total fluorescence intensity of the accumulated YFP-DNA-PK_{CS} was ∼2.5-fold (7/2.8) higher after microirradiation with the 365-nm laser than after irradiation with the 800-nm laser. From this, we infer that our microirradiation protocol induces between 2,500 and 3,700 DSBs (2.5 × 1,000 and 2.5 × 1,500, respectively) at the beam-focus of our pulsed 365-nm laser.

Irradiation with uranium-charged particles

V3 cells, expressing YFP-tagged DNA-PK_{CS}, were irradiated with uranium particles with an initial energy of 11.4 MeV/nucleon (energy on the target cells, 3.8 MeV/nucleon) at the UNILAC facility at GSI, as previously described (Jakob et al., 2000). Cells were cultured in a Petri dish on 40-μm-thick polycarbonate sheets. Duration of irradiation was <5 ms per sample. Kinetic measurements of the recruitment of YFP-DNA-PK_{CS} at sites of ion traversals were performed using a beamline microscope (Jakob et al., 2005) equipped with a 7190–53 EBCCD-camera (Hamamatsu). Uranium ion tracks were visualized by etching polycarbonate, as described previously (Jakob et al., 2005).

Time-lapse imaging and calculation of protein recruitment kinetics

During microirradiation and time-lapse imaging, cells were maintained in CO_2-independent medium (Invitrogen) at 37°C. Images were made with an Axiovert 200M microscope, equipped with an AxioCam HRm, using a Plan-Apochromat 63×/NA 1.40 oil immersion objective. Time-lapse image acquisition was started before laser microirradiation to obtain an image of the unirradiated cell. DSBs were introduced in cell nuclei by microirradiation with our pulsed nitrogen laser (see Laser microirradiation and imaging) at the time of the third image. Exposure time was set at 400 ms, allowing 4 laser pulses to hit a defined region of a single nucleus. All images before and after irradiation were captured with a 400-ms exposure time. Signal intensities of accumulated YFP at the microirradiated site were converted into a numerical value by the use of the Carl Zeiss Axiovision software version 4.5. To compensate for nonspecific fluorescence bleaching during the repeated image acquisition, the fluorescence intensity of an undamaged region was subtracted from the fluorescence intensity of the accumulation spot for each cell at each time point. Relative fluorescence (RF) was calculated by the following formula: $RF_{(t)} = (I_t - I_{preIR})/(I_{max} - I_{preIR})$, where I_{preIR} is the fluorescence intensity of the microirradiated region before irradiation, and I_{max} represents the maximum fluorescence signal in the microirradiated region.

Photobleaching

FRAP measurements were performed by photobleaching the entire DNA-PK_{CS} accumulation spot that formed after introduction of DSBs and by measuring the subsequent recovery of fluorescence signal in that region. Imaging and FRAP measurements were performed on an LSM 510 Meta confocal microscope using a Plan-Apochromat 63×/NA 1.40 oil immersion objective. Images were acquired by scanning with the 514-nm line of the argon laser of the LSM 510 Meta microscope using the standard image acquisition function of the LSM 510 software version 4.0SP1. The tube current of the argon laser was set at 6.1 A, and the laser intensity was set at 0.3%. The pinhole was set at 2.51 Airy units, corresponding to an optical slice of 1.9 μm. DSBs were introduced in the nuclei of cultured cells by microirradiation with the pulsed nitrogen laser (see Laser microirradiation and imaging). Cells were cultured in 35-mm glass-bottom dishes. During measurements, cells were maintained in a CO_2-independent medium (Invitrogen) at 37°C. FRAP measurements were initiated 10 min after the introduction of DSBs, when maximum accumulation of DNA-PK_{CS} was observed. A photobleaching pulse was given at 100% laser intensity (514 nm line of an argon laser, tube current set at 6.1 A). The dimensions of the circular FRAP area matched those of the accumulation spot ($\sim$1.7 μm^2) and were kept constant during all measurements. An image of the nucleus was taken before photobleaching, immediately after photobleaching and at 30-s time intervals for 600 s. In every image, we measured the average fluorescence of the photobleached accumulation spot (F_{as}), from which the background fluorescence intensity was subtracted. Subsequently, F_{as} was normalized to the prebleach value: $F_{norm} = F_{as}(t) / F_{as}(0)$.

Online supplemental material

Fig. S1 shows the cellular expression of WT, 7A, and KD DNA-PK_{CS}, as verified by Western blot analysis. In addition, it demonstrates that complementing V3 cells with YFP-tagged DNA-PK_{CS} reduces the radiation-sensitivity of the V3 cells to the level of AA8 cells. Fig. S2 shows the cellular expression of Ku80 in Ku80-complemented Xrs6 cells, as verified by Western blot analysis and in vivo immunostaining. It also demonstrates that complementing Xrs6 cells with Ku80 reduces the radiation-sensitivity of the Xrs6 cells to the level of AA8 cells. Finally, it demonstrates by Western blot analysis that phosphorylation of the Ser-2056 residue of DNA-PK_{CS} is a Ku80-dependent process. Fig. S3 shows the cellular expression of WT, S2056A, and T2609A DNA-PK_{CS}, as verified by Western blot analysis. The online version of this article is available at http://www.jcb.org/cgi/content/full/jcb.200608077/DC1.

We would like to thank Nicole S. Verkaik (Erasmus Medical Center) and Jason Kirk (Carl Zeiss MicroImaging, Inc.) for technical assistance, Megan C. Ayers for valued administrative support, and Dr. Michael D. Story for critical revision of the manuscript.

This work was supported by National Institutes of Health (5-R37-CA050519-16 and PO1-CA92584), the National Aeronautics and Space Association (NNA05CM04G and NNJ05HD36G), and the European Union (project RISC-RAD; contract number FI6R-CT-2003-508842).

Submitted: 14 August 2006
Accepted: 20 March 2007

References

Bekker-Jensen, S., C. Lukas, R. kitagawa, F. Melander, M.B. Kastan, J. Bartek, and J. Lukas. 2006. Spatial organization of the mammalian genome surveillance machinery in response to DNA strand breaks. *J. Cell Biol.* 173:195–206.

Block, W.D., Y. Yu, D. Merkle, J.L. Gifford, Q. Ding, K. Meek, and S.P. Lees-Miller. 2004. Autophosphorylation-dependent remodeling of the DNA-dependent protein kinase catalytic subunit regulates ligation of DNA ends. *Nucleic Acids Res.* 32:4351–4357.

Calsou, P., P. Frit, O. Humbert, C. Muller, D.J. Chen, and B. Salles. 1999. The DNA-dependent protein kinase catalytic activity regulates DNA end processing by means of Ku entry into DNA. *J. Biol. Chem.* 274:7848–7856.

Chan, D.W., B.P. Chen, S. Prithivirajsingh, A. Kurimasa, M.D. Story, J. Qin, and D.J. Chen. 2002. Autophosphorylation of the DNA-dependent protein kinase catalytic subunit is required for rejoining of DNA double-strand breaks. *Genes Dev.* 16:2333–2338.

Chen, B.P., D.W. Chan, J. Kobayashi, S. Burma, A. Asaithamby, K. Morotomi-Yano, E. Botvinick, J. Qin, and D.J. Chen. 2005. Cell cycle dependence of DNA-dependent protein kinase phosphorylation in response to DNA double strand breaks. *J. Biol. Chem.* 280:14709–14715.

Chen, B.P., N. Uematsu, J. Kobayashi, Y. Lerenthal, A. Krempler, H. Yajima, M. Lobrich, Y. Shiloh, and D.J. Chen. 2007. Ataxia telangiectasia mutated (ATM) is essential for DNA-PKcs phosphorylations at the Thr-2609 cluster upon DNA double strand break. *J. Biol. Chem.* 2007:6582–6587.

Chen, F., S.R. Peterson, M.D. Story, and D.J. Chen. 1996. Disruption of DNA-PK in Ku80 mutant xrs-6 and the implications in DNA double-strand break repair. *Mutat. Res.* 362:9–19.

Critchlow, S.E., and S.P. Jackson. 1998. DNA end-joining: from yeast to man. *Trends Biochem. Sci.* 23:394–398.

Cui, X., Y. Yu, S. Gupta, Y.M. Cho, S.P. Lees-Miller, and K. Meek. 2005. Autophosphorylation of DNA-dependent protein kinase regulates DNA end processing and may also alter double-strand break repair pathway choice. *Mol. Cell. Biol.* 25:10842–10852.

Denekamp, J., G.F. Whitmore, and P. Jeggo. 1989. Biphasic survival curves for XRS radiosensitive cells: subpopulations or transient expression of repair competence? *Int. J. Radiat. Biol.* 55:605–617.

Ding, Q., Y.V. Reddy, W. Wang, T. Woods, P. Douglas, D.A. Ramsden, S.P. Lees-Miller, and K. Meek. 2003. Autophosphorylation of the catalytic subunit of the DNA-dependent protein kinase is required for efficient end processing during DNA double-strand break repair. *Mol. Cell. Biol.* 23:5836–5848.

Douglas, P., G.P. Sapkota, N. Morrice, Y. Yu, A.A. Goodarzi, D. Merkle, K. Meek, D.R. Alessi, and S.P. Lees-Miller. 2002. Identification of in vitro and in vivo phosphorylation sites in the catalytic subunit of the DNA-dependent protein kinase. *Biochem. J.* 368:243–251.

Falck, J., J. Coates, and S.P. Jackson. 2005. Conserved modes of recruitment of ATM, ATR and DNA-PKcs to sites of DNA damage. *Nature*. 434:605–611.

Goodarzi, A.A., Y. Yu, E. Riballo, P. Douglas, S.A. Walker, R. Ye, C. Harer, C. Marchetti, N. Morrice, P.A. Jeggo, and S.P. Lees-Miller. 2006. DNA-PK autophosphorylation facilitates Artemis endonuclease activity. *EMBO J.* 25:3880–3889.

Hammarsten, O., and G. Chu. 1998. DNA-dependent protein kinase: DNA binding and activation in the absence of Ku. *Proc. Natl. Acad. Sci. USA*. 95:525–530.

Jakob, B., M. Scholz, and G. Taucher-Scholz. 2000. Immediate localized CDKN1A (p21) radiation response after damage produced by heavy-ion tracks. *Radiat. Res.* 154:398–405.

Jakob, B., J.H. Rudolph, N. Gueven, M.F. Lavin, and G. Taucher-Scholz. 2005. Live cell imaging of heavy-ion-induced radiation responses by beamline microscopy. *Radiat. Res.* 163:681–690.

Kanaar, R., J.H. Hoeijmakers, and D.C. van Gent. 1998. Molecular mechanisms of DNA double strand break repair. *Trends Cell Biol.* 8:483–489.

Kienker, L.J., E.K. Shin, and K. Meek. 2000. Both V(D)J recombination and radioresistance require DNA-PK kinase activity, though minimal levels suffice for V(D)J recombination. *Nucleic Acids Res.* 28:2752–2761.

Kim, J.S., T.B. Krasieva, H. Kurumizaka, D.J. Chen, A.M.R. Taylor, and K. Yokomori. 2005. Independent and sequential recruitment of NHEJ and HR factors to DNA damage sites in mammalian cells. *J. Cell Biol.* 170:341–347.

Kurimasa, A., S. Kumano, N.V. Boubnov, M.D. Story, C.S. Tung, S.R. Peterson, and D.J. Chen. 1999. Requirement for the kinase activity of human DNA-dependent protein kinase catalytic subunit in DNA strand break rejoining. *Mol. Cell. Biol.* 19:3877–3884.

Lan, L., S. Nakajima, Y. Oohata, M. Takao, S. Okano, M. Masutani, S.H. Wilson, and A. Yasui. 2004. In situ analysis of repair processes for

oxidative DNA damage in mammalian cells. *Proc. Natl. Acad. Sci. USA*. 101:13738–13743.

Lan, L., S. Nakajima, K. Komatsu, A. Nussenzweig, A. Shimamoto, J. Oshima, and A. Yasui. 2005. Accumulation of Werner protein at DNA double-strand breaks in human cells. *J. Cell Sci.* 118:4153–4162.

Lees-Miller, S.P., and K. Meek. 2003. Repair of DNA double strand breaks by non-homologous end joining. *Biochimie*. 85:1161–1173.

Li, Z., T. Otevrel, Y. Gao, H.L. Cheng, B. Seed, T.D. Stamato, G.E. Taccioli, and F.W. Alt. 1995. The XRCC4 gene encodes a novel protein involved in DNA double-strand break repair and V(D)J recombination. *Cell*. 83:1079–1089.

Lieber, M.R., Y. Ma, U. Pannicke, and K. Schwarz. 2003. Mechanism and regulation of human non-homologous DNA end-joining. *Nat. Rev. Mol. Cell Biol.* 4:712–720.

Mari, P.O., B.I. Florea, S.P. Persengiev, N.S. Verkaik, H.T. Bruggenwirth, M. Modesti, G. Giglia-Mari, K. Bezstarosti, J.A. Demmers, T.M. Luider, et al. 2006. Dynamic assembly of end-joining complexes requires interaction between Ku70/80 and XRCC4. *Proc. Natl. Acad. Sci. USA*. 103:18597–18602.

Merkle, D., P. Douglas, G.B. Moorhead, Z. Leonenko, Y. Yu, D. Cramb, D.P. Bazett-Jones, and S.P. Lees-Miller. 2002. The DNA-dependent protein kinase interacts with DNA to form a protein-DNA complex that is disrupted by phosphorylation. *Biochemistry*. 41:12706–12714.

Reddy, Y.V., Q. Ding, S.P. Lees-Miller, K. Meek, and D.A. Ramsden. 2004. Non-homologous end joining requires that the DNA-PK complex undergo an autophosphorylation-dependent rearrangement at DNA ends. *J. Biol. Chem.* 279:39408–39413.

Singleton, B.K., M.I. Torres-Arzayus, S.T. Rottinghaus, G.E. Taccioli, and P.A. Jeggo. 1999. The C terminus of Ku80 activates the DNA-dependent protein kinase catalytic subunit. *Mol. Cell. Biol.* 19:3267–3277.

Smith, G.C., and S.P. Jackson. 1999. The DNA-dependent protein kinase. *Genes Dev.* 13:916–934.

Soubeyrand, S., L. Pope, B. Pakuts, and R.J. Hache. 2003. Threonines 2638/2647 in DNA-PK are essential for cellular resistance to ionizing radiation. *Cancer Res.* 63:1198–1201.

van Gent, D.C., J.H. Hoeijmakers, and R. Kanaar. 2001. Chromosomal stability and the DNA double-stranded break connection. *Nat. Rev. Genet.* 2:196–206.

Weterings, E., and D.C. van Gent. 2004. The mechanism of non-homologous end-joining: a synopsis of synapsis. *DNA Repair (Amst.)*. 3:1425–1435.

Weterings, E., N.S. Verkaik, H.T. Bruggenwirth, J.H. Hoeijmakers, and D.C. van Gent. 2003. The role of DNA dependent protein kinase in synapsis of DNA ends. *Nucleic Acids Res.* 31:7238–7246.

Whitmore, G.F., A.J. Varghese, and S. Gulyas. 1989. Cell cycle responses of two X-ray sensitive mutants defective in DNA repair. *Int. J. Radiat. Biol.* 56:657–665.

Yajima, H., K.J. Lee, and B.P. Chen. 2006. ATR-dependent phosphorylation of DNA-dependent protein kinase catalytic subunit in response to UV-induced replication stress. *Mol. Cell. Biol.* 26:7520–7528.